Article:
McRae, M.P., Kerr, A.R., Janal, M.N. et al. (2021) Nuclear F-actin cytology in oral dysplasia and oral squamous cell carcinoma. Journal of Dental Research, 100 (5). pp. 479-486. ISSN: 0022-0345

https://doi.org/10.1177/0022034520973162

McRae MP, Kerr AR, Janal MN, et al. Nuclear F-actin Cytology in Oral Epithelial Dysplasia and Oral Squamous Cell Carcinoma. Journal of Dental Research. 2021;100(5):479-486.

DOI: 10.1177/0022034520973162.

Nuclear F-actin Cytology in Oral Dysplasia and Oral Squamous Cell Carcinoma

Authors

1. Michael P. McRae, Ph.D.
   Department of Biomaterials, Bioengineering Institute, New York University, New York, NY, USA
   michael.mcrae@nyu.edu
2. A. Ross Kerr, D.D.S.
   Department of Oral and Maxillofacial Pathology, Radiology & Medicine, New York University College of Dentistry, New York, NY, USA
   ark3@nyu.edu
3. Malvin N. Janal, Ph.D.
   Department of Epidemiology and Health Promotion, New York University College of Dentistry, New York, NY, USA
   mj62@nyu.edu
4. Martin H. Thornhill, Ph.D.
   Department of Oral & Maxillofacial Medicine, Surgery and Pathology, School of Clinical Dentistry, University of Sheffield, Sheffield, UK
   M.Thornhill@sheffield.ac.uk
5. Spencer W. Redding, D.D.S.
   Department of Comprehensive Dentistry and Mays Cancer Center, The University of Texas Health Science Center at San Antonio, San Antonio, TX, USA
   redding@uthscsa.edu
6. Nadarajah Vigneswaran, D.M.D.
   Department of Diagnostic and Biomedical Sciences, The University of Texas Health Science Center at Houston, Houston, TX, USA
   Nadarajah.Vigneswaran@uth.tmc.edu
7. Stella K. Kang, M.D.
   Departments of Radiology, Population Health New York University School of Medicine, New York, NY, USA
   stella.kang@nyulangone.org
8. Richard Niederman, D.M.D.
   Department of Epidemiology and Health Promotion, New York University, New York, NY, USA
   rniederman@nyu.edu
9. Nicolaos J. Christodoulides, Ph.D.
   Department of Biomaterials, Bioengineering Institute, New York University, New York, NY, USA
   nicolaoschristo19@gmail.com
10. Denise A. Trochesset, D.D.S.
    Department of Oral and Maxillofacial Pathology, Radiology & Medicine, New York University College of Dentistry, New York, NY, USA
    dat5@nyu.edu
11. Craig Murdoch, Ph.D.
    Department of Oral & Maxillofacial Medicine, Surgery and Pathology, School of Clinical Dentistry, University of Sheffield, Sheffield, UK
    c.murdoch@sheffield.ac.uk

12. Isaac Dapkins, M.D.
    Departments of Population Health and Medicine, New York University School of Medicine, New York, NY, USA
    Isaac.Dapkins@nyulangone.org
13. H. Stanley McGuff, D.D.S.
    Department of Pathology, The University of Texas Health Science Center at San Antonio, San Antonio, TX, USA
    mcguff@uthscsa.edu
14. Jerry Bouquot, D.D.S.
    Department of Diagnostic and Biomedical Sciences, The University of Texas School of Dentistry at Houston, Houston, TX, USA
    Jerry.Bouquot@uth.tmc.edu
15. Sayli S. Modak, M.S.
    Department of Biomaterials, Bioengineering Institute, New York University, New York, NY, USA
    sayli.modak@nyu.edu
16. Glennon W. Simmons, B.S.
    Department of Biomaterials, Bioengineering Institute, New York University, New York, NY, USA
    glennon.simmons@nyu.edu
17. John T. McDevitt, Ph.D.
    Chair, Department of Biomaterials, Bioengineering Institute, New York University, New York, NY, USA
    mcdevitt@nyu.edu

Corresponding Author: John T. McDevitt, Ph.D., Chair, Department of Biomaterials, Bioengineering Institute, New York University, 433 First Avenue, Room 820, New York, NY 10010-4086, USA. Email: mcdevitt@nyu.edu. Phone: 212-998-9204.

Keywords: artificial intelligence; biomarkers; point-of-care testing; single-cell analysis; squamous cell carcinoma; actin

Abstract

Oral cavity cancer has a low 5-year survival rate, but improved outcomes occur when the disease is detected early. Cytology is a less invasive method to assess potentially malignant oral lesions relative to the gold-standard scalpel biopsy and histopathology. We aimed to assess the diagnostic accuracy of a cytological test for analysis of the entire spectrum of oral epithelial dysplasia and oral squamous cell carcinoma. We enrolled subjects with potentially malignant oral lesions, previously diagnosed malignant lesions, and healthy volunteers without lesions. We obtained brush cytology specimens and matched scalpel biopsies for all subjects with lesions. Histopathological assessment of the scalpel biopsy specimens classified lesions into six categories. Brush cytology specimens from 486 subjects were assessed relative to histopathology using phenotypic and molecular markers. Machine learning classifiers were trained to identify cytological features of potential clinical utility. Multimodal diagnostic models were developed using cytology results, lesion characteristics, and risk factors. Cytological features substantially outperformed lesion appearance and risk factors in predicting dysplasia and squamous cell carcinoma. Squamous cells with nuclear F-actin staining were associated with early disease (i.e., distinguishing benign lesions from more severe lesions), while small round parabasal-like cells and leukocytes were associated with late disease (i.e., distinguishing severe dysplasia and carcinoma from less severe lesions). Lesions with the impression of oral lichen planus demonstrated a strong protective effect in both early and late disease prediction. Diagnostic models accurately discriminated early and late disease with AUCs of 0.82 (95% CI 0.77–0.87) and 0.93 (0.88–0.97), respectively. The cytological features identified here have the potential to serve as predictors for lesion screening and surveillance of the entire spectrum of oral epithelial dysplasia and squamous cell carcinoma in multiple care settings.

Introduction

Potentially malignant oral lesions (PMOL), such as leukoplakia or erythroplakia, are clinical diagnoses rendered when a clinician encounters a white, mixed red-white, or red patch that cannot be attributed to a benign etiology. These lesions require further diagnostic testing to rule out oral epithelial dysplasia (OED) or oral squamous cell carcinoma (OSCC). The typical pathway to diagnosis of PMOL is biopsy and histopathologic evaluation requiring an invasive surgical procedure and specialty referral. Given the overlapping clinical features of oral epithelial lesions encountered by primary care clinicians, such as dentists, it is challenging to perform an adequate risk assessment of oral epithelial lesions based on appearance and risk factors alone and decide if referral is required (Lingen et al. 2017). While there are numerous minimally invasive adjuncts to assist in the triage of PMOL, only cytology has been demonstrated as an accurate surrogate for histopathology (Huber 2018; Lingen et al. 2017; Rashid and Warnakulasuriya 2015). However, delays associated with remote laboratory testing and significant bias of previous studies (Poate et al. 2004; Svirsky et al. 2002) have hindered the adoption of oral cytology adjuncts. There is a strong need for adjunctive testing in near real-time at the point of care (POC) with sufficient sensitivity to identify at-risk lesions and sufficient specificity to discriminate benign lesions from those with increasing risk of malignancy.

Cytological signatures are morphological, phenotypical, or intensity-based measurements from images of stained cells which may be of clinical and diagnostic utility. Cell phenotypic changes involving cytoskeletal actin have been associated with cancer initiation and progression (Gunning et al. 2008; Stevenson et al. 2012). Cancer cells require a high degree of cellular motility to invade, spread, and grow—processes that are driven by actin polymerization, cell adhesion, and actin-myosin contraction (Olson and Sahai 2009). Actin content has shown strong promise as a biomarker for OSCC (de Jong et al. 2010). Previous studies have implicated nuclear actin in a

variety of functions, such as supporting and organizing nuclear content (Belin et al. 2013), mechanosensing (Le et al. 2016), nuclear expansion (Moore and Vartiainen 2017), and increasing nuclear compliance while maintaining mechanical protection for genetic material (Miroshnikova et al. 2017). Early studies of *in vitro* cellular transformation models showed promise for nuclear actin biomarkers in uroepithelial cell lines (Hemstreet et al. 1996). While promising basic scientific research has advanced the understanding of such cytological signatures, their translational diagnostic utility has not yet been demonstrated for OED or OSCC. Multimodal models incorporating cytological signatures including actin, features of lesion appearance, and risk factors have strong potential to improve diagnostic performance.

We previously reported a cytology-on-a-chip system comprising microfluidics, multispectral fluorescence imaging, and single-cell analytics (Weigum et al. 2010). A multisite clinical validation effort led to the development of one of the largest oral cytology databases for PMOL (Abram et al. 2016) in which brush cytology measurements were prospectively collected, measured, and correlated with six levels of histopathological diagnosis (Speight et al. 2015). The same approach demonstrated strong potential for surveillance of OSCC in Fanconi Anemia patients (Abram et al. 2018). Recently, we developed a POC oral cytology tool comprising a brush cytology test kit, cartridge, instrument, clinical algorithms, and software that automates cellular and molecular analysis of various cytological signatures of OED and OSCC in a matter of minutes (McRae et al. 2020). Although diagnostic accuracy for the cytology-on-a-chip rivaled and exceeded commercially available adjuncts, more studies were needed to investigate the clinical utility of novel cytological signatures of OED and OSCC. In this current study, we describe an analysis of new cytological signatures of OED and OSCC using cytology results from our previous study. We asked whether new multimodal diagnostic signatures, including cytological features related to F-actin localization, could predict OED and OSCC in clinical applications such as PMOL triage in primary care and OED/OSCC surveillance in secondary or tertiary care settings.

Materials and Methods

Study design and participants

Previously, a cytology-on-a-chip system was evaluated for its ability to classify mucosal lesions according to histopathologic diagnosis in a four-site, international, prospective, non-interventional study (Abram et al. 2016; Speight et al. 2015). The study was approved by the Institutional Review Boards of all participating institutions, including Rice University, where chip-based measurements were completed on brush cytology samples. All patients provided written informed consent. Histopathological and brush cytological samples were collected from three groups: (1) prospectively recruited patients with PMOL who underwent scalpel biopsy as part of standard of care, (2) patients with recently diagnosed OSCC, and (3) healthy volunteers without lesions. Histopathological diagnosis categorized scalpel biopsy specimens into six categories based on the WHO guidelines (El-Naggar et al. 2017) plus healthy controls without lesions who did not undergo scalpel biopsy and histopathology. A new adjudication process (Speight et al. 2015) was implemented to overcome limitations of conventional OED grading which is often considered subjective and lacking intra- and inter-observer reproducibility (Warnakulasuriya et al. 2008). Adjacent serial histologic sections were independently scored by two pathologists. Upon disagreement of scoring, a third independent pathologist reviewed both sections. If the adjudicator did not agree with either of the initial two pathologists, a third stage consensus review was conducted to attain a final diagnosis. This process was able to achieve 100% agreement compared to an initial pre-adjudication rate of 69.9%. The current study utilized cytological measurements from this prior work (Abram et al. 2016; Speight et al. 2015). All subjects with sufficient material and complete biomarker results were included in the analysis.

Procedures

Brush cytological specimens were collected and processed as previously described (Abram et al. 2016; Speight et al. 2015). Complete details are provided in the **Appendix**. All subjects underwent brush sampling of the oral lesion, site of known cancerous lesion, or clinically normal mucosa. All assays contained Phalloidin-AlexaFluor-647 for cytoplasmic counterstaining and visualizing F-actin localization and DAPI for nuclear counterstaining in the secondary antibody cocktail. Image analysis software CellProfiler (Carpenter et al. 2006) detected individual cells; defined nuclear and cytoplasmic boundaries; obtained intensity measurements for red (F-actin), green (immunofluorescence), and blue (DNA) spectral channels; and defined morphometric parameters.

Cell phenotype classifier

Trained and tested cell phenotype classifiers quantified the distributions of cellular and nuclear phenotypes. The cell phenotype classifier was trained to identify differentiated squamous epithelial (DSE) cells, small round (SR) cells, mononuclear leukocytes (ML), and lone nuclei (LN). This work introduces new nuclear phenotypes and a classifier for DSE cells with (NA+) and without (NA-) nuclear F-actin (i.e., cells with or without F-actin localized in or around the nucleus). Both cellular and nuclear *k*-Nearest Neighbor algorithms were trained on a subset of 144 cellular/nuclear features from cytology, including morphological and biomarker intensity-based measurements. Principal component analysis was performed on the training set to improve data visualization. Histopathological gradings were coded as follows: (1) normal/no lesion, (2) benign, (3) mild dysplasia, (4) moderate dysplasia, (5) severe dysplasia or carcinoma *in situ*, and (6) malignant/OSCC. The cell phenotyping algorithms were applied across all cytological measurements, and the proportions of each phenotype were compared for each lesion class.

Model development and statistical analysis

Detailed methods are provided in the **Appendix**. Diagnostic accuracy (area under the curve [AUC], sensitivity, and specificity) was determined between various histopathology gradings with case *vs* non-case, as indicated by "|", including models for early and late disease. Here, *early disease* was defined as the distinction of cases with benign lesions from all other more severe lesions (i.e., 2 | 3,4,5,6), and *late disease* was defined as the distinction of cases with lesions of moderate severity from all more severe lesions (i.e., 2,3,4 | 5,6). Univariate and multivariate adjusted odds ratios (OR), 95% confidence intervals, and p-values (two-tailed) were calculated from logistic regression analyses. Pre- and post-test probabilities were estimated by likelihood ratios for late disease. The predictors included cell phenotype percentages for types NA-, NA+, SR, and ML ($\log_{10}$ transformed); sex; age (10-year increments); lesion area ($\log_{10}$ transformed); lesion color (red, white, or red and white); clinical impression of oral lichen planus; and smoking pack years ($\log_{10}$ transformed). Lasso logistic regression models were developed, and model responses were evaluated for diagnostic performance.

Results

A total of 486 subjects with histopathology-matched brush cytology measurements were included in the analysis. **Table 1** shows the characteristics and histopathological diagnoses and **Appendix Figure 1** summarizes subject accrual. The analysis of each subject considered approximately 2000 cells and 150 biomarker intensity and morphology-based parameters. All measurements

were completed with cytology-on-a-chip prototypes that have recently been translated to POC cartridges and instruments (**Appendix Figure 2**) (McRae et al. 2020).

Cell phenotype classifiers were trained to identify five distinct cellular/nuclear phenotypes (**Figure 1A**). The differentiated squamous epithelial cells or mature keratinocytes (DSE cells) were broad/flat cells 50-100 µm in diameter with low NC ratio and low cytoplasmic F-actin staining intensity. These cells were further differentiated by the presence (NA+) or absence (NA-) of F-actin localized within or surrounding the nucleus. Immature basaloid keratinocytes (SR cells) were small circular cells 12-30 µm in diameter with high NC ratio and strong cytoplasmic F-actin staining intensity. Mononuclear leukocytes (ML) appeared as small, brightly stained pink objects 6-23 µm in diameter. Lone nuclei without a cytoplasm (LN) were objects with DAPI counterstaining, but no cytoplasmic F-actin staining, approximately 5-12 µm in diameter.

The latent variable structure of the data was explored with principal components (PC) analysis. Scatter plots show that the data varied along three dimensions of cell size (PC1), cytoplasmic F-actin (PC2), and nuclear F-actin (PC3) (**Figure 1B** and **1C**). These PCs account for 33%, 15%, and 14% variance, respectively, and suggest that cell size and nuclear F-actin content/distribution may play an important role in distinguishing cell phenotypes. The cross-validated *k*-nearest neighbors algorithm for the cellular phenotypes resulted in overall accuracy of 98.5% and accuracy of 100%, 95.1%, 97.4%, and 100% for DSE, SR, ML, and LN, respectively. Similarly for the DSE nuclear phenotypes, the overall accuracy was 97.6% with 99.0% and 95.6% accuracy for types NA+ and NA-, respectively. Cell phenotype distributions varied with lesion severity (**Figure 2**). In cases with more advanced disease, NA- cells decreased, and SR and ML cells increased (Wilcoxon rank sum test, $p<0.05$). The fraction of NA+ cells increased with disease severity ($p<0.05$) for all diagnostic categories except normal *vs* benign ($p=0.53$).

Logistic regression models were developed to discriminate between early and late disease splits (**Appendix Table 1**). Early disease refers to the distinction of cases with benign lesions from all other more severe lesions, while late disease refers to the distinction of cases with lesions of moderate severity from all more severe lesions. The NA- cells showed a strong protective effect (i.e., OR<1) in both early and late disease univariate models. Similarly, the clinical impression of oral lichen planus was associated with 85-90% reduction in the odds of high-grade OED and OSCC. Multivariate models showed some confounding among the predictors. Unique contributors to the early disease model included the presence of NA+ cells, age, and lichen planus. Unique contributors to the late disease model included the presence of SR and ML cells, sex, lesion color, and lesions with the clinical impression of oral lichen planus. These data highlight the unique contribution of cytological analysis to differentiating histopathologically-verified diagnoses of OED and OSCC.

Diagnostic performance of a multimodal model was evaluated for various diagnostic cutoffs (**Table 2**). These predictors included: cell phenotype distributions, age, sex, smoking pack years, lesion area, clinical impression of lesion as oral lichen planus, and lesion color (white, red, or both red and white). The lasso logistic regression model responses were numerical values between 0 and 100, and model accuracy was determined at a cutoff value that maximized AUC. All models assigned the right diagnosis to at least 82% of the sample. Late disease models were more accurate than early disease models. The best models properly assigned 95% of the cases.

The improvement in accuracy attributable to the late disease modeling can be summarized by comparing pre- and post-test likelihood ratios (Akobeng 2007). **Figure 3** (**and Appendix Table 2**) shows the conditional post-test probability for distinguishing patients with late disease as a function of pre-test probability for patients with presence (solid lines) or absence (dashed lines)

of clinical risk factors in the multivariate model. The multivariate model showed the greatest change in post-test probabilities, as indicated by the outermost band of both groups of ellipses. Among the univariate predictors, NA- cells (negative), SR cells (positive), and ML cells (positive) were strongly related to the disease state. Lesions with a white-colored appearance showed a strong protective effect (i.e., the probability of severe dysplasia or OSCC was significantly reduced for those presenting with homogeneous leukoplakia).

Discussion

In the current study reveals the relative importance of cytological and clinical variables in predicting early and late disease. We found that cell phenotype distributions from cytology are strong predictors of disease. Significantly, we observed that different cell phenotypes were more important for distinguishing early *vs* late disease. As expected, SR and ML cells were found to indicate late disease. Small circular cells resembling SR cells were previously found to increase in frequency with OED severity (Babshet et al. 2011). Strong evidence for the association between chronic inflammation and carcinogenesis has been reported previously, which supports the result of elevated numbers of leukocytes in high grade OED and OSCC (Tampa et al. 2018).

Interestingly, the proportion of NA+ cells was a statistically significant factor in predicting early disease. The current study is the first to link increased proportions of nuclear F-actin cells with early OED (see **Appendix** for literature review details). It is possible that differentiated squamous cells that develop thick perinuclear/nuclear F-actin formations could represent transitional phenotypes embodying a morphological transformation from NA+ to SR. More studies would be needed to (1) explore the relationships between phenotypes, (2) investigate whether phalloidin-F-actin staining on NA+ cells reflects binding to nuclear *vs* perinuclear F-actin, (3) visualize subnuclear F-actin features, and (4) advance the understanding of cell phenotypic changes in malignant transformation.

In addition to cell phenotypes, six immunofluorescence targets were selected based on their capacity to distinguish benign, dysplastic, and malignant oral epithelial cells and were investigated in the current study. However, we found that the discriminatory ability of these immunofluorescence targets was inferior relative to that acquired using the cell phenotypes featured here. The sole biomarker-based exception was nuclear F-actin, which demonstrated superior disease discrimination.

Multivariate and multimodal models combining cell phenotypes from cytology, lesion characteristics, and traditional risk factors yielded higher diagnostic utility than any individual predictor. Cytological signatures substantially outperformed clinical features (lesion appearance and risk factors) in predicting OED and OSCC. While lesion color was a significant factor in late disease, it was less useful in distinguishing lesions with low malignant potential that are more commonly observed in primary care settings. Although traditional risk factors like tobacco use did not play a dominant role for distinguishing any OED/OSCC model, smoking pack years was statistically significant in a 2 *vs* 6 model with OR (95% CI) of 1.97 (1.02–3.97). This result further highlights the challenge of lesion diagnosis in a realistic population of patients presenting with intermediate histopathological grading as opposed to extreme comparisons (e.g., healthy control *vs* cancer) commonly found in the literature. The clinical impression of oral lichen planus demonstrated a strong protective effect in both early and late disease prediction. Motivated by this result, plans are now in progress to develop a cytological test for lichen planus in primary care settings where the condition may be overlooked or misdiagnosed.

Today, remote laboratory cytology services require long delays between sample collection, shipment, and obtaining the test results, prolonging patient anxiety and delaying the referral of patients with high-risk lesions to specialist care settings. By contrast, a POC test could deliver cytology test results within the same visit.

Prior studies of cytology adjuncts had significant methodological gaps. By only performing matched gold-standard histopathology on a subset of lesions with a higher index of suspicion for malignancy, these studies did not account for lesions with a lower index of suspicion which are more regularly encountered in primary care settings (Poate et al. 2004; Sciubba 1999). These tests frequently returned an ambiguous “atypical” result (Svirsky et al. 2002). Similarly, many studies of adjuncts only compare normal or benign *vs* malignant lesions and exclude a full range of dysplastic lesions, leading to overly optimistic results. For example, an oral rinse adjunctive test evaluated control subjects without lesions *vs* oral cancer subjects (1 *vs* 6) with an AUC of 0.76 (Pereira et al. 2016). In the current study, the cytology-on-a-chip approach was assessed relative to six diagnostic levels of histopathology. As might be expected, earlier disease was more difficult to differentiate than late disease in the current study (AUCs of 0.82 *vs* 0.93). Likewise, if dysplastic lesions are excluded from the current analysis, the diagnostic performance becomes optimistic (AUCs of 0.97 and 0.95 for 1 *vs* 6 and 2 *vs* 6, respectively). Although there was a small proportion of false negative results warranting further investigation, these results were consistent with the imperfection of oral cancer related diagnostic adjuncts and suggest that persistent mucosal lesions may necessitate subsequent resampling.

One limitation for the current study is that lesions were evaluated by expert clinicians in secondary care settings where the prevalence of high-grade OED and OSCC would be higher than in primary care. Further, subjects met strict inclusion criteria which may reflect a narrower spectrum of lesions than might be clinically diagnosed as PMOLs in a primary care setting. Since prevalence of high-grade OED and OSCC is expected to be substantially lower in primary care settings, future studies are needed to evaluate the diagnostic performance of PMOLs detected there. Although the diagnostic models described here were tuned to optimize AUC and, thus, balanced sensitivity and specificity, future implementations may select different cutoffs based on intended use (e.g., a diagnostic test for ruling in, with high specificity, high-grade OED/OSCC in secondary or tertiary care settings or a screening test for ruling out, with high sensitivity, clinically evident but benign lesions in primary care settings).

In closing, this multimodal, POC-compatible cytology-on-a-chip approach has the potential to be used as an oral lesion precision diagnostic across the OED/OSCC disease spectrum and in various patient settings. Primary care clinicians typically do not have the information needed to effectively differentiate the significance of oral mucosal lesions. This automated cytology platform will help primary care clinicians perform a more accurate and real-time risk stratification of lesions, allowing them to make appropriate referrals. In secondary or tertiary care settings, the cytological signatures of patients with a history of OED and OSCC may be monitored longitudinally and have the potential to identify progression and malignant transformation/recurrence earlier, and less invasively, than current surveillance approaches. It is also feasible that this diagnostic may be further developed to identify unique cytological signatures for other mucosal diseases, whether immune (e.g., lichen planus) or pathogen-mediated (e.g., candidal leukoplakia). Plans are now in place to evaluate the POC oral cytology tool in a clinical trial to validate and assess diagnostic performance *vs* routine care in primary care clinics. Additional plans are in place to follow high risk patients longitudinally for malignant transformation and cancer recurrence in secondary or tertiary surveillance settings.

Author Contributions

M.P. McRae contributed to conception, design, data acquisition, analysis, and interpretation, drafted and critically revised the manuscript; A.R. Kerr, M.H. Thornhill, S.W. Redding, and N. Vigneswaran contributed to design, data acquisition and interpretation, critically revised the manuscript; M. Janal, S.K. Kang, and R. Niederman contributed to analysis and interpretation, critically revised the manuscript; N.J. Christodoulides, D.A. Trochesset, C. Murdoch, I. Dapkins, H.S. McGuff, J. Bouquot, S.S. Modak, and G.W. Simmons critically revised the manuscript; J.T. McDevitt contributed to conception, design, data acquisition, analysis, and interpretation, drafted and critically revised the manuscript. All authors gave final approval and agree to be accountable for all aspects of the work.

Acknowledgements

Research reported in this publication was supported by the National Institute of Dental and Craniofacial Research Division of the National Institutes of Health (1RC2DE020785-01, 4R44DE025798-02, and R01DE024392) with a portion of the funding being derived from Renaissance Health Service Corporation and Delta Dental of Michigan. Rho Inc., a contract research organization (Chapel Hill, NC, USA), provided statistical, regulatory, data management and clinical monitoring support, as well as operational management. The content of this manuscript is solely the responsibility of the authors and does not necessarily represent the official views of the National Institutes of Health. The authors thank the University of Texas Health Science Center at San Antonio (UTHSCSA) (Stephanie Rowan, Chih-Ko Yeh, Frank Miller), University of Texas Health Science Center at Houston (UTHSCH) (Nagi Demian, Etan Weinstock, Nancy Bass), New York University / Bluestone Center for Clinical Research (Joan Phelan, Patricia Corby, Ismael Khouly), Sheffield Teaching Hospitals NHS Foundation Trust and the University of Sheffield (Paul Speight, Christine Freeman, Anne Hegarty, Katy D'Apice) for assistance in obtaining and pathological evaluation of clinical samples. The authors also thank Rho, Inc. (Chapel Hill, North Carolina) (Julie Vick) for assisting with patient data management and (Robert James) for statistical and data analysis support. Finally, the authors thank Shannon Weigum, Pierre Floriano, and Timothy J. Abram for early contributions to the project, including assay development and database organization. M.P. McRae has served as a paid consultant for SensoDx and has a provisional patent pending. G.W. Simmons has patents US10060937B2 and US7781226B2 issued. D.A. Trochesset has received grants from the New York University College of Dentistry for work performed as part of the current study. M.H. Thornhill has received National Institutes of Health grant 1RC2DE020785-01 for work performed as part of the current study. S.W. Redding has patent US9535068B2 issued. S.K. Kang has received royalties from Wolters Kluwer for work performed outside of the current study. J.T. McDevitt has received grants from the National Institutes of Health for work performed as part of the current study (grants 1RC2DE020785-01, 4R44DE025798-02, and R01DE024392) and has a provisional patent pending. In addition, he has an ownership position and an equity interest in SensoDx II LLC and serves on its Scientific Advisory Board. All other authors declare no potential conflicts of interest with respect to the authorship and/or publication of this article

Figures and Tables

Table 1. Subject characteristics. Histopathological diagnoses were based on the WHO classification (El-Naggar et al. 2017). Average pack years is the average number of cigarettes smoked per day times years smoked divided by 20 (interquartile range). Histopathological diagnoses were coded 1-6 as referenced throughout this manuscript.

	N (%)
Total	486
Sex	
Male	211 (43.4)
Female	275 (56.6)
Age	
≤ 60	321 (66.0)
> 60	165 (34.0)
Tobacco	
Never	213 (43.8)
Any Tobacco Use	273 (56.2)
Previous Smokers	140 (28.8)
Current Smokers	113 (23.3)
Average Pack Years in Tobacco Users	13 (1.8–30.0)
Subject Group	
Healthy Volunteer	121 (24.9)
Patients with Previously Diagnosed Malignant Lesion	36 (7.4)
Patients with a Potentially Malignant Lesion	329 (67.7)
Histopathological Diagnosis	
1 - Normal	121 (24.9)
2 - Benign	241 (49.6)
3 - Mild Dysplasia	38 (7.8)
4 - Moderate Dysplasia	12 (2.5)
5 - Severe Dysplasia	9 (1.9)
6 - Malignant	65 (13.4)

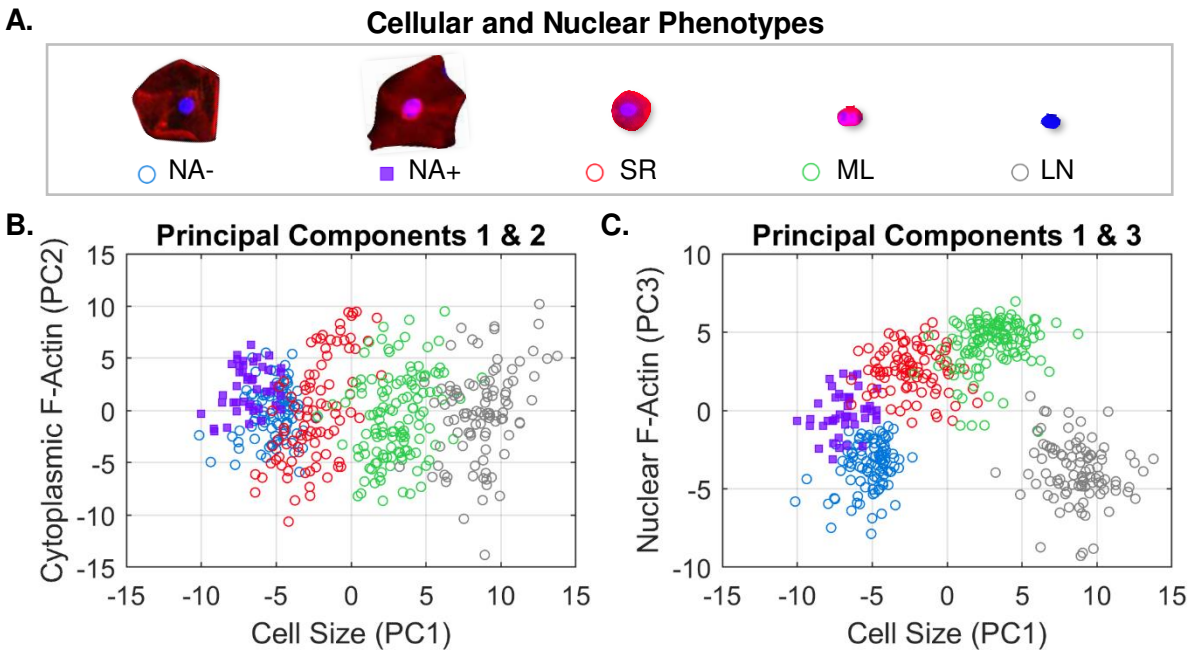

Figure 1. Development of cellular and nuclear phenotype models. Machine learning classifiers were developed to identify five phenotypes (A). Principal component analysis of cellular phenotypes show substantial separation between cellular phenotype labels for PC1 *vs* PC2 (B) and PC1 *vs* PC3 (C), with the majority of the variance explained by cell size (PC1), cytoplasm F-actin (PC2), and nuclear F-actin (PC3). NA- cells are differentiated squamous cells without nuclear F-actin. NA+ cells are differentiated squamous cells with nuclear F-actin. SR cells are small round cells. ML are mononuclear leukocytes. LN are lone nuclei. PC is the principal component.

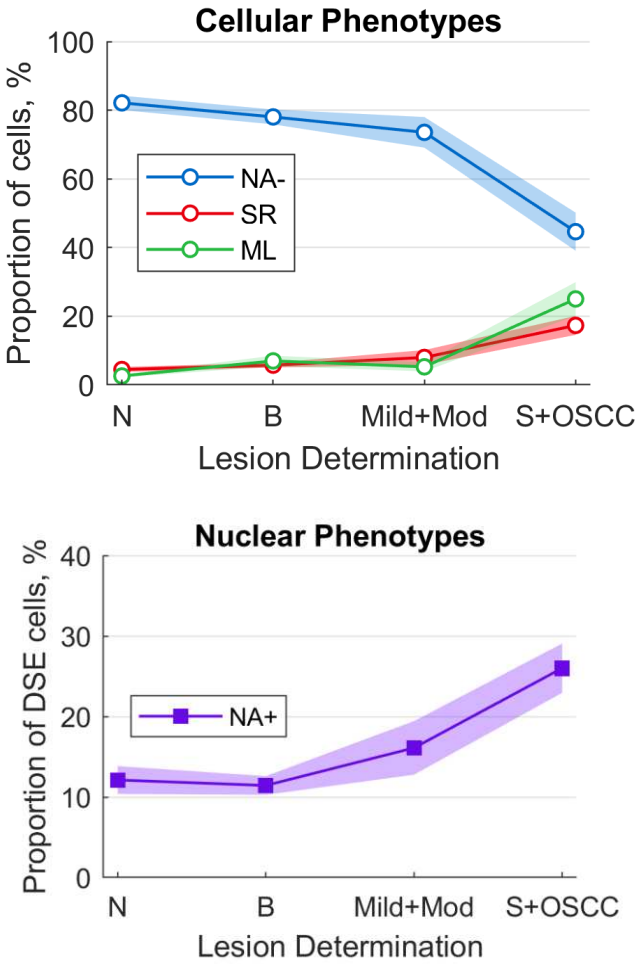

Figure 2. Application of cellular and nuclear phenotype models. Distributions of NA-, SR, and ML cells (top) within the study population, representing the predicted mean cell type percentages and 95% CI within each lesion class. Distribution of NA+ cells out of all DSE cells (bottom). DSE cells are differentiated squamous epithelial cells. N is normal lesion (n=121). B is benign lesion (n=241). Mild+Mod is mild and moderate dysplasia (n=50). S+OSCC is severe and oral squamous cell carcinoma (n=74).

Table 2. OED spectrum diagnostic models. Sensitivity, specificity, and AUC (95% CIs) are shown for the cross-validated dichotomous algorithms for early disease (2 | 3,4,5,6), mild | moderate dysplasia (2,3 | 4,5,6), low | high risk (2,3,4L | 4H,5,6), late disease (2,3,4 | 5,6), benign *vs* malignant (2 *vs* 6), and healthy control *vs* malignant (1 *vs* 6) models.

	Sensitivity	**Specificity**	**AUC**
Early Disease - 2 | 3,4,5,6	0.72 (0.67–0.76)	0.73 (0.69–0.78)	0.82 (0.77–0.87)
2,3 | 4,5,6	0.79 (0.74–0.83)	0.85 (0.81–0.89)	0.89 (0.84–0.93)
2,3,4L | 4H,5,6	0.80 (0.75–0.84)	0.82 (0.78–0.86)	0.89 (0.84–0.93)
Late Disease - 2,3,4 | 5,6	0.86 (0.82–0.90)	0.84 (0.80–0.88)	0.93 (0.88–0.97)
2 *vs* 6	0.89 (0.85–0.92)	0.90 (0.85–0.93)	0.95 (0.91–0.98)
1 *vs* 6	0.94 (0.89–0.97)	0.92 (0.87–0.95)	0.97 (0.94–1.00)

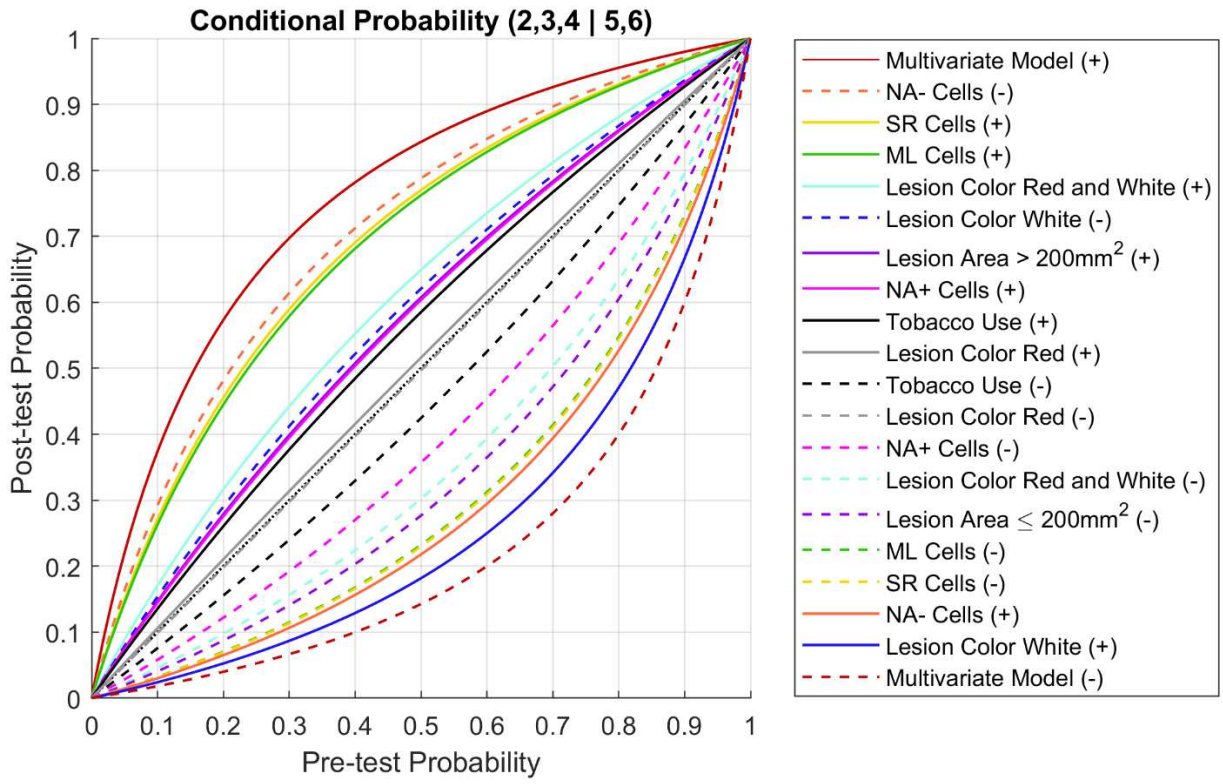

Figure 3. Pre- and post-test probability. Conditional probability plot for late disease (2,3,4 | 5,6). Post-test probabilities are plotted as a function of pre-test probability for patients with positive (solid lines) and negative (dashed lines) indications for clinical risk factors (lesion color, lesion area, smoking), cellular phenotypes, and the multivariate model.

References

Abram TJ, Floriano PN, Christodoulides N, James R, Kerr AR, Thornhill MH, Redding SW, Vigneswaran N, Speight PM, Vick J et al. 2016. 'cytology-on-a-chip' based sensors for monitoring of potentially malignant oral lesions. Oral Oncol. 60:103-111.

Abram TJ, Pickering CR, Lang AK, Bass NE, Raja R, Meena C, Alousi AM, Myers JN, McDevitt JT, Gillenwater AM et al. 2018. Risk stratification of oral potentially malignant disorders in fanconi anemia patients using autofluorescence imaging and cytology-on-a chip assay. Transl Oncol. 11(2):477-486.

Akobeng AK. 2007. Understanding diagnostic tests 2: Likelihood ratios, pre- and post-test probabilities and their use in clinical practice. Acta Paediatrica. 96(4):487-491.

Babshet M, Nandimath K, Pervatikar S, Naikmasur V. 2011. Efficacy of oral brush cytology in the evaluation of the oral premalignant and malignant lesions. Journal of Cytology. 28(4):165-172.

Belin BJ, Cimini BA, Blackburn EH, Mullins RD. 2013. Visualization of actin filaments and monomers in somatic cell nuclei. Molecular Biology of the Cell. 24(7):982-994.

Carpenter AE, Jones TR, Lamprecht MR, Clarke C, Kang IH, Friman O, Guertin DA, Chang JH, Lindquist RA, Moffat J et al. 2006. Cellprofiler: Image analysis software for identifying and quantifying cell phenotypes. Genome Biol. 7(10):R100.

de Jong EP, Xie H, Onsongo G, Stone MD, Chen X-B, Kooren JA, Refsland EW, Griffin RJ, Ondrey FG, Wu B et al. 2010. Quantitative proteomics reveals myosin and actin as promising saliva biomarkers for distinguishing pre-malignant and malignant oral lesions. PLOS ONE. 5(6):e11148.

El-Naggar AK, Chan JK, Grandis JR, Takata T, Slootweg PJ. 2017. Who classification of tumours of the head and neck. El-Naggar AKC, J. K. C., Grandis JR, Takata T, Slootweg PJ, editors. Lyon: IARC Press.

Gunning P, O'Neill G, Hardeman E. 2008. Tropomyosin-based regulation of the actin cytoskeleton in time and space. Physiol Rev. 88(1):1-35.

Hemstreet GP, 3rd, Rao J, Hurst RE, Bonner RB, Waliszewski P, Grossman HB, Liebert M, Bane BL. 1996. G-actin as a risk factor and modulatable endpoint for cancer chemoprevention trials. J Cell Biochem Suppl. 25:197-204.

Huber MA. 2018. Adjunctive diagnostic techniques for oral and oropharyngeal cancer discovery. Dent Clin North Am. 62(1):59-75.

Le HQ, Ghatak S, Yeung C-YC, Tellkamp F, Günschmann C, Dieterich C, Yeroslaviz A, Habermann B, Pombo A, Niessen CM et al. 2016. Mechanical regulation of transcription controls polycomb-mediated gene silencing during lineage commitment. Nat Cell Biol. 18(8):864-875.

Lingen MW, Abt E, Agrawal N, Chaturvedi AK, Cohen E, D'Souza G, Gurenlian J, Kalmar JR, Kerr AR, Lambert PM et al. 2017. Evidence-based clinical practice guideline for the evaluation of potentially malignant disorders in the oral cavity: A report of the american dental association. J Am Dent Assoc. 148(10):712-727.

McRae MP, Modak SS, Simmons GW, Trochesset DA, Kerr AR, Thornhill MH, Redding SW, Vigneswaran N, Kang SK, Christodoulides NJ et al. 2020. Point-of-care oral cytology tool for the screening and assessment of potentially malignant oral lesions. Cancer Cytopathol.

Miroshnikova YA, Nava MM, Wickström SA. 2017. Emerging roles of mechanical forces in chromatin regulation. J Cell Sci. 130(14):2243.

Moore HM, Vartiainen MK. 2017. F-actin organizes the nucleus. Nat Cell Biol. 19:1386.

Olson MF, Sahai E. 2009. The actin cytoskeleton in cancer cell motility. Clin Exp Metastasis. 26(4):273-287.

Pereira LHM, Reis IM, Reategui EP, Gordon C, Saint-Victor S, Duncan R, Gomez C, Bayers S, Fisher P, Perez A et al. 2016. Risk stratification system for oral cancer screening. Cancer Prev Res. 9(6):445.

Poate TWJ, Buchanan JAG, Hodgson TA, Speight PM, Barrett AW, Moles DR, Scully C, Porter SR. 2004. An audit of the efficacy of the oral brush biopsy technique in a specialist oral medicine unit. Oral Oncol. 40(8):829-834.

Rashid A, Warnakulasuriya S. 2015. The use of light-based (optical) detection systems as adjuncts in the detection of oral cancer and oral potentially malignant disorders: A systematic review. J Oral Pathol Med. 44(5):307-328.

Sciubba JJ. 1999. Improving detection of precancerous and cancerous oral lesions: Computer-assisted analysis of the oral brush biopsy. J Am Dent Assoc. 130(10):1445-1457.

Speight PM, Abram TJ, Floriano PN, James R, Vick J, Thornhill MH, Murdoch C, Freeman C, Hegarty AM, D'Apice K et al. 2015. Interobserver agreement in dysplasia grading: Toward an enhanced gold standard for clinical pathology trials. Oral Surg Oral Med Oral Pathol Oral Radiol. 120(4):474-482.

Stevenson RP, Veltman D, Machesky LM. 2012. Actin-bundling proteins in cancer progression at a glance. J Cell Sci. 125(5):1073.

Svirsky JA, Burns JC, Carpenter WM, Cohen DM, Bhattacharyya I, Fantasia JE, Lederman DA, Lynch DP, Sciubba JJ, Zunt SL. 2002. Comparison of computer-assisted brush biopsy results with follow up scalpel biopsy and histology. Gen Dent. 50(6):500-503.

Tampa M, Mitran MI, Mitran CI, Sarbu MI, Matei C, Nicolae I, Caruntu A, Tocut SM, Popa MI, Caruntu C et al. 2018. Mediators of inflammation - a potential source of biomarkers in oral squamous cell carcinoma. Journal of Immunology Research. 2018:12.

Torres-Rendon A, Roy S, Craig GT, Speight PM. 2009. Expression of mcm2, geminin and ki67 in normal oral mucosa, oral epithelial dysplasias and their corresponding squamous-cell carcinomas. Br J Cancer. 100(7):1128-1134.

Vigneswaran N, Beckers S, Waigel S, Mensah J, Wu J, Mo J, Fleisher KE, Bouquot J, Sacks PG, Zacharias W. 2006. Increased emmprin (cd 147) expression during oral carcinogenesis. Exp Mol Pathol. 80(2):147-159.

Warnakulasuriya S, Reibel J, Bouquot J, Dabelsteen E. 2008. Oral epithelial dysplasia classification systems: Predictive value, utility, weaknesses and scope for improvement. J Oral Pathol Med. 37(3):127-133.

Weigum SE, Floriano PN, Redding SW, Yeh C, Westbrook SD, McGuff HS, Lin A, Miller FR, Villarreal F, Rowan SD et al. 2010. Nano-bio-chip sensor platform for examination of oral exfoliative cytology. Cancer Prev Res. 3(4):518-528.

Nuclear F-actin Cytology in Oral Dysplasia and Oral Squamous Cell Carcinoma

M.P. McRae, A.R. Kerr, M.N. Janal, M.H. Thornhill, S.W. Redding, N. Vigneswaran, S.K. Kang, R. Niederman, N.J. Christodoulides, D.A. Trochesset, C. Murdoch, I. Dapkins, H.S. McGuff, J. Bouquot, S.S. Modak, G.W. Simmons, and J.T. McDevitt

APPENDIX

Study Participants

The data used in this study originated from a 1053-patient study which aimed to assess the diagnostic accuracy of this cytology-on-a-chip system relative to scalpel biopsy and histopathology. The methods and preliminary results of this original study were published previously (Abram et al. 2016; Speight et al. 2015). **Figure S1** shows the criteria for subject inclusion/exclusion for the current study, which is a re-analysis of the same data collected previously. Subjects from three groups consented to enrollment of the original study. Of those 1053 subjects, 54 withdrew from the study and, thus, cytology measurements were not recorded. Of the 999 remaining enrolled subjects for the original study, 513 were not eligible for the current study due to the following reasons: partial cytology measurements (n=21); inadequate number of cells in the sample (n=47); samples were used for other purposes (n=2); samples were lost due to shipping errors and/or freezer failures (n=44); cytology results were not measured due to funding constraints or missing (n=399). All the remaining 486 subjects with complete cytology data were included in the current analysis.

Clinical Protocol

The clinical protocol for this study was published previously (Speight et al. 2015) and is summarized as follows. Patients in group 1 underwent brush sampling of the oral lesion and a brush sampling of the contralateral, clinically normal mucosa. The brush cytology sample was taken immediately before the same lesion underwent a scalpel biopsy. Patients in group 2 underwent brush biopsy of the known cancerous lesion, as well as the contralateral, clinically normal mucosa. For healthy volunteers in group 3, a brush biopsy of normal appearing tissue on the lateral or ventral surface of the tongue and a brush biopsy of normal appearing tissue on the left or right buccal mucosa were taken. Brush biopsy samples were taken using a soft Rovers

Orcellex oral cytology brush (Rovers Medical Devices B.V., Oss, The Netherlands). The brush was applied directly to the lesion or control oral mucosa using mild pressure and rotated 360 degrees approximately 10-15 times in the same direction to obtain the cytologic sample. Histopathological specimens were examined and coded as follows: (1) normal/no lesion, (2) benign, (3) mild dysplasia, (4) moderate dysplasia, (5) severe dysplasia or carcinoma *in situ*, and (6) malignant/OSCC.

Cytology-on-a-Chip Protocol

The following methods have been published previously (Abram et al. 2016) and are summarized here. Immediately after brush cytology samples were collected, cells were harvested by vortexing the brush head in minimum essential medium (MEM) culture media, followed by a PBS wash, re-suspension in FBS containing 10% of the cryo-preservative dimethyl-sulfoxide (DMSO), frozen, and stored in a -80°C freezer. Prior to processing on the device, patient samples were thawed rapidly in a 37°C water bath, washed with PBS, and fixed for one hour in 0.5% formaldehyde prepared fresh from a 16% stock solution (Polysciences, Warrington, PA, #18814-20). After fixation, cells were washed twice in PBS, re-suspended in 150µL 0.1% PBS with 0.1% BSA (PBSA), and stored at 40°C until ready to process. Before sample delivery, the cell suspension was diluted in a 20% glycerol/0.1% PBSA solution to improve cell distribution across the membrane and to reduce cell clumping. Using a custom built manifold connecting external fluidic tubing to the inlet and outlet ports of the microfluidic device, the assembly was positioned on a robotically controlled microscope stage (ProScan II, Prior Scientific, Cambridge, UK) and connected to a peristaltic pump (SciQ 400, Watson Marlow, Wilmington, MA) and manually controlled 6-position injector valve (Vici, Valco Instruments, Houston, TX). Antibody stock solutions were vortexed for 30 seconds and centrifuged at 14,000rpm for five minutes before preparing working dilutions to avoid precipitates. All assays contained Phalloidin and DAPI in the secondary antibody cocktail, but each was specific for a single molecular biomarker primary-secondary antibody pair. Working dilutions of antibodies were prepared in 0.1% PBSA with 0.1% Tween-20 (EMD Millipore, Billerica, MA, # 655206). Primary monoclonal antibodies were raised from either mouse (EGFR [Life Technologies, Carlsbad, CA, #MS-378-P, 10µg/mL]), rabbit (αvβ6 [Abcam, Cambridge, MA, #Ab124968, 6µg/mL], Ki67 [Abcam #Ab15580, 29µg/mL], and MCM2 [Abcam #Ab108935, 10µg/mL]), or goat (CD-147 [EMMPRIN] [R&D Systems, Minneapolis, MN, #AF972, 20µg/mL]. AlexaFluor-488 conjugated secondary antibodies were specific for F $(ab')_2$ fragments of mouse IgG (Life Technologies #A11017, 20µg/mL for EFGR), rabbit IgG (Life

Technologies #A11070, 50µg/mL for αvβ6, 64µg/mL for Ki67, and 23.5µg/mL for MCM2), or goat IgG (Life Technologies #A11078, 40µg/mL for CD147). A working concentration of 0.33µM was used for Phalloidin-AlexaFluor-647 (Life Technologies #A22287) and 5µM for DAPI (Life Technologies #D3571).

In summary, the lab-on-a-chip sample processing was comprised of the following steps: 1) the device was primed with PBS at a flow rate of 735µL/min for two minutes, 2) the cell suspension in 20% glycerol/0.1% PBSA was delivered at 1.5mL/min for two minutes, 3) cells were washed with PBS at 1mL/min for 2.5min, 4) the primary antibody solution was delivered through a 0.2µm PVDF syringe filter at 250µL/min for 2.5min, 5) a wash step similar to step 3 was performed, 6) the secondary antibody solution was delivered under the same conditions as step 4, 7) a final wash step was performed, and 8) automated image capture was performed.

Sample Digitization

More complete details on cytology sample digitization and a complete list of intensity and morphological parameters can be found in our previous publication (Abram et al. 2016). Images were recorded with a motorized reflected fluorescence microscope (Olympus BX-RFAA) equipped with a CCD camera (Hamamatsu ORCA-03G) through a 10x objective (10x/0.30NA UPlanFl, Olympus). A total of 25 unique fields of view repeated for three different z-focal planes were automatically captured across a 20mm^2 area using a robotic x-y-z microscope stage. Due to the complex three-dimensional morphology of oral squamous cells, multiple z-focal planes were captured and subsequently combined into a single, enhanced depth-of-field image to simplify the multi-spectral detection of the three fluorescent labels using ImageJ “stack focuser”. Combinations of custom macros and the open-source image analysis tools ImageJ (Schneider et al. 2012) and CellProfiler (Carpenter et al. 2006) were developed to automatically detect individual cells and define their nuclear and cytoplasmic boundaries as individual regions of interest (ROI). These ROIs were used to obtain intensity measurements associated with the three spectral channels and were used to define morphometric parameters. The DAPI and Phalloidin molecular labels served primarily to assist in the automated segmentation of individual nuclei and cytoplasm, respectively.

Cell Identification Model Training and Validation

A cell type classification model was explored for its ability to discriminate and quantitate the frequency and distributions of four cell types: differentiated squamous epithelial (DSE) cells, small round (SR) cells, mononuclear leukocytes (ML), and lone nuclei (LN). An additional model further classified DSE cells according to nuclear phenotypes for cells with (NA+) and without (NA-) nuclear F-actin (i.e., cells with or without F-actin localized in or around the nucleus). Both cellular and nuclear algorithms were trained on a subset of 144 cellular/nuclear features from cytology, including morphological and biomarker intensity-based measurements. A training set was manually compiled by randomly selecting and labeling cells, resulting in approximately 100-200 single-cell objects for each of the cell types. All features were log-normalized and standardized for zero mean and unit variance. Principal component analysis was performed on the training set, and scatterplots of the principal components were generated to visualize the internal data structure and variance. A *k*-nearest neighbors (*k*-NN) classifier was trained on the standardized features using 10-fold cross-validation and configured to find the nearest seven neighbors in feature space (Euclidean distance). Cross-validated predicted responses by the *k*-NN classifier were recorded, and accuracy was reported for the overall cross-validation set and individually for each of the cell types. *k*-NN model responses with four or less out of seven similar neighbors were labelled “unknown” type, and cross-validated accuracy was reported for the overall training set after accounting for unknown object types. The classification models were retrained on the entire training dataset, and this final model was applied to the study population and averaged across each of the six molecular biomarker assays. Plots were generated to show the distributions of cell phenotypes across diagnostic categories as follows: 121 normal/non-neoplastic, 241 benign, 59 dysplasia, and 65 malignant. Median values of cell phenotypes were compared for all lesion determinations using a two-sided Wilcoxon rank sum test at a significance level of $p = 0.05$. Cell phenotype frequencies and distributions for each subject were retained for use in clinical algorithm development.

Lasso Logistic Regression Models

The analysis of dichotomous outcomes with mutually exclusive levels is common in clinical diagnostics, and logistic regression is regarded as the standard method of analysis for these situations attributed to its probabilistic interpretation and ability to function as a dichotomous classifier. Clinical data are often challenged by high-dimensionality and highly correlated predictors that may generate model coefficients with high variance. For these situations, a size penalty as implemented by the lasso technique may be applied to shrink the effect sizes and reduce coefficient variability. Additionally, the lasso technique performs automatic parameter

selection by eliminating predictors with less importance. In high-dimensional data sets, reducing the set of predictors often leads to better prediction performance and generalizability and has shown improvements over manual stepwise selection methods. This lasso logistic regression model is suited to our platform because it is inherently more intuitive than previous methods which consider hundreds of measurements from cytology that are difficult to interpret. A lasso logistic regression approach was used to prevent overfitting, reduce coefficient variability, and retain a sparse model with improved generalizability and interpretability. Diagnostic accuracy (area under the curve [AUC], sensitivity, and specificity) for several models was determined between various histopathology gradings with case *vs* non-case, as indicated by "|". Only subjects with evaluable data for all biomarker measurements and potentially malignant oral lesion (PMOL) status were considered. The results from six molecular biomarker assays on the cytology-on-a-chip system were pooled to obtain final estimates. Non-zero lasso logistic regression coefficients were retained for the following predictors: NA+, NA-, SR, ML, age, sex, smoking pack years, lesion area, lichen planus, and lesion color (**Table S3**). AUC, sensitivity, and specificity were reported as mean and 95% confidence interval values for the cross-validated test set.

Literature Review

We reviewed prior diagnostic studies on PubMed using the search terms "(nuclear OR nucleus) F-actin AND cancer" using the narrow filter. The search returned 17 studies with only one study investigating nuclear F-actin in cell lines (Hemstreet et al. 1996). There were no previous studies that evaluated nuclear F-actin as a clinical cancer diagnostic biomarker. We also reviewed the literature for previous studies of oral cancer adjuncts (Huber 2018; Lingen et al. 2017; Rashid and Warnakulasuriya 2015). Many adjunct study designs were biased. For example, studies only performed matched gold-standard histopathology on a subset of subjects with a higher index of suspicion for malignancy, effectively ignoring lesions with a lower index of suspicion which are more regularly encountered in primary care settings (Poate et al. 2004; Sciubba 1999). One prominent adjunct frequently returned an ambiguous "atypical" result (Svirsky et al. 2002). Another study only evaluated control subjects without lesions and oral cancer subjects, leading to overly optimistic results by excluding subjects with dysplasia (Pereira et al. 2016). Further, most cytological tests were conducted at remote laboratories, resulting in significant delays between sample collection and test results.

Figures and Tables

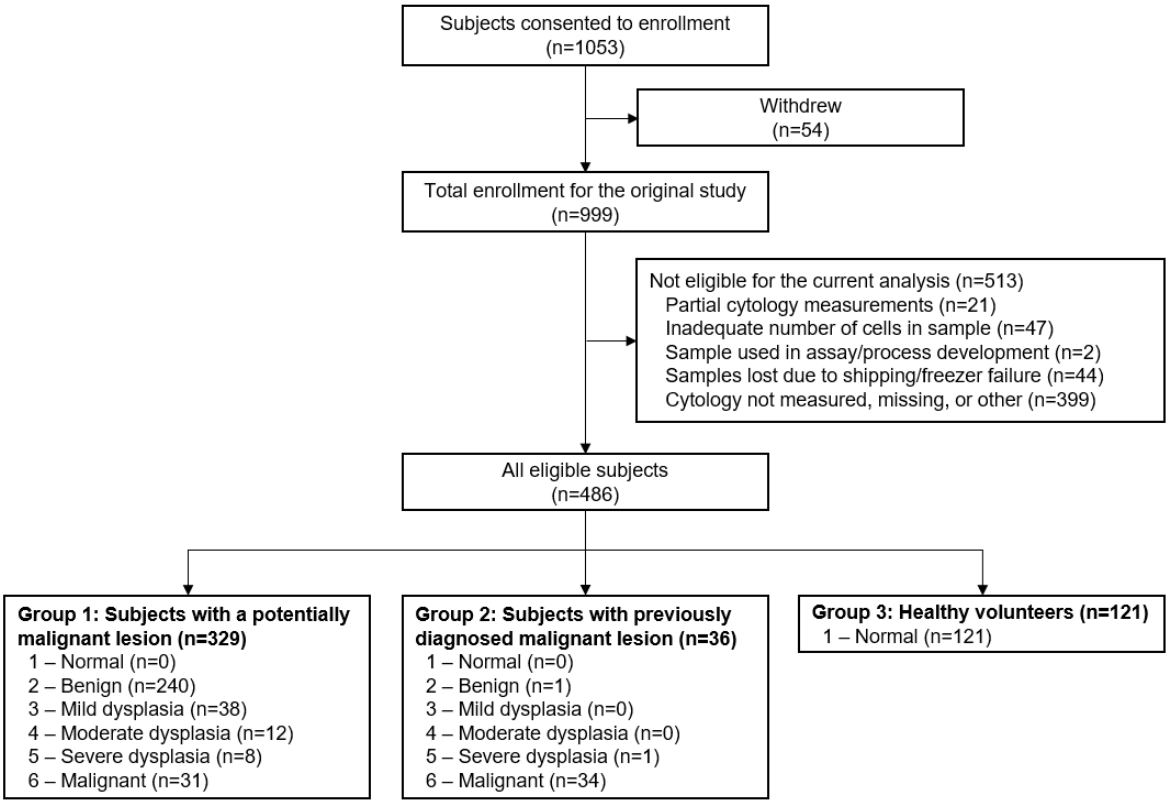

Appendix Figure 1. Study participants

A total of 1053 subjects from each of the three groups consented to enrollment of the original study. Of those 1053 subjects, 54 withdrew from the study and, thus, cytology measurements were not recorded. Of the 999 remaining enrolled subjects for the original study, 513 were not eligible for the current study due to the following reasons: partial cytology measurements (n=21); inadequate number of cells in the sample (n=47); samples were used for other purposes (n=2); samples were lost due to shipping errors and/or freezer failures (n=44); cytology results were not measured due to funding constraints or missing (n=399). All the remaining 486 subjects with complete cytology data were included in the current analysis.

Appendix Figure 2. The Point-of-Care Oral Cytology Tool

The point-of-care (POC) oral cytology tool allows for the cellular analysis of minimally invasive brush biopsy samples. The cell suspension collected in this manner allows for the simultaneous quantification of cell morphometric data and expression of molecular biomarkers of malignant potential in an automated manner using refined image analysis algorithms based on pattern recognition techniques and advanced statistical methods. This novel approach turns around biopsy results in a matter of minutes as compared to days for traditional pathology methods, thereby making it amenable to POC settings. The POC testing is expected to have tremendous implications in the rapid management of patient disease by enabling dental practitioners and primary care physicians to circumvent the need for multiple referrals and consultations before obtaining assessment of molecular risk of PMOL.

Appendix Table 1. Odds ratios

	Early Disease (2 | 3,4,5,6)				Late Disease (2,3,4 | 5,6)			
	Univariate OR	**p**	**Multi-variate OR**	**p**	**Univariate OR**	**p**	**Multi-variate OR**	**p**
NA+ cells	4.79 (2.45–9.74)	< 0.001	2.97 (1.22–7.41)	0.018	4.09 (1.86–9.44)	< 0.001	2.85 (0.76–11.16)	0.124
NA- cells	0.01 (0.002–0.04)	< 0.001	0.22 (0.03–1.16)	0.087	0.002 (0.0004–0.01)	< 0.001	0.28 (0.03–2.09)	0.231
SR cells	8.84 (4.94–16.54)	< 0.001	2.30 (0.97–5.58)	0.060	28.48 (12.48–71.69)	< 0.001	4.68 (1.34–17.50)	0.018
ML cells	4.45 (2.86–7.11)	< 0.001	1.65 (0.75–3.67)	0.215	13.77 (7.50–26.90)	< 0.001	4.03 (1.33–12.87)	0.015
Sex	1.76 (1.14–2.74)	0.011	1.58 (0.90–2.81)	0.112	2.65 (1.56–4.61)	< 0.001	4.23 (1.92–9.81)	< 0.001
Age	1.18 (1.00–1.39)	0.048	1.24 (1.02–1.51)	0.037	1.20 (0.99–1.45)	0.065	1.36 (1.04–1.81)	0.026
Lesion area	1.48 (1.23–1.84)	< 0.001	1.11 (0.90–1.39)	0.340	2.31 (1.61–3.52)	< 0.001	1.21 (0.89–1.75)	0.258
Lesion color	-	-	-	-	-	-	-	-
White	ref.	-	ref.	-	ref.	-	ref.	-
Red	1.14 (0.56–2.27)	0.703	0.63 (0.26–1.47)	0.294	5.14 (1.95–14.59)	0.001	2.81 (0.77–10.63)	0.119
Red and white	2.10 (1.30–3.44)	0.003	1.59 (0.84–3.03)	0.153	9.02 (4.20–22.43)	< 0.001	6.95 (2.58–21.21)	< 0.001
Lichen planus	0.13 (0.06–0.25)	< 0.001	0.16 (0.07–0.36)	< 0.001	0.08 (0.02–0.23)	< 0.001	0.12 (0.03–0.41)	0.002
Pack years	1.64 (1.20–2.23)	0.002	1.40 (0.94–2.09)	0.095	1.60 (1.12–2.29)	0.010	1.35 (0.78–2.33)	0.285

Odds ratios (95% confidence intervals) from univariate and multivariate logistic regression for early disease late disease models. The following predictors were $\log_{10}$ transformed: NA+, NA-, SR, and ML cells, lesion area, pack years. Sex corresponds to male (i.e., male=1, female=0). Age is in 10-year increments. Lichen planus is the clinical impression of lichen planus.

Appendix Table 2. Likelihood ratios

	Early Disease (2 | 3,4,5,6)		Late Disease (2,3,4 | 5,6)	
Predictor	**LR +**	**LR -**	**LR +**	**LR -**
Multivariate Model	2.70 (2.33–3.13)	0.38 (0.33–0.45)	5.59 (4.77–6.56)	0.16 (0.14–0.19)
NA- Cells	0.52 (0.38–0.72)	2.62 (1.90–3.59)	0.27 (0.16–0.45)	3.80 (2.29–6.30)
NA+ Cells	1.63 (1.38–1.94)	0.50 (0.42–0.60)	1.53 (1.20–1.93)	0.55 (0.43–0.70)
SR Cells	2.03 (1.74–2.38)	0.41 (0.35–0.48)	3.30 (2.71–4.00)	0.30 (0.25–0.36)
ML Cells	1.85 (1.56–2.20)	0.52 (0.44–0.61)	3.16 (2.59–3.84)	0.30 (0.25–0.37)
Lesion Color				
Red and White	1.43 (1.18–1.74)	0.71 (0.58–0.86)	1.88 (1.51–2.35)	0.42 (0.34–0.53)
White	0.68 (0.50–0.92)	1.24 (0.92–1.67)	0.21 (0.10–0.43)	1.66 (0.80–3.43)
Red	0.78 (0.51–1.19)	1.04 (0.69–1.59)	1.07 (0.65–1.78)	0.99 (0.60–1.64)
Lesion Area	1.44 (1.21–1.72)	0.53 (0.45–0.63)	1.55 (1.24–1.93)	0.38 (0.30–0.47)
Tobacco Use	1.44 (1.18–1.76)	0.74 (0.61–0.91)	1.41 (1.08–1.85)	0.73 (0.56–0.96)
Alcohol Use	0.87 (0.68–1.10)	1.25 (0.99–1.58)	0.82 (0.60–1.10)	1.34 (0.99–1.81)
Alcohol and Tobacco Use	1.35 (1.06–1.71)	0.87 (0.69–1.11)	1.22 (0.86–1.71)	0.91 (0.65–1.28)

Positive and negative likelihood ratios (95% CI) for clinical and cytological predictors in distinguishing early disease and late disease. LR+ is the positive likelihood ratio. LR- is the negative likelihood ratio. Lesion area positive was defined as patients with lesion area > 200 mm^2. Tobacco positive was defined as patients with smoking pack years > 2.5 pack years. Alcohol use positive was defined as patients having 12 or more drinks in the past year. Alcohol and tobacco positive was defined as patients with both tobacco use and alcohol use.

Table S3. Predictor definitions.

Abbreviation	Description
NA-	percentage of differentiated squamous epithelial cells without nuclear F-actin (i.e., number of NA- cells divided by total cells, where 'total cells' is the number of cells of type NA-, NA+, SR, and ML)
NA+	percentage of differentiated squamous cells with nuclear F-actin (i.e., number of NA+ cells divided by total cells, where 'total cells' is the number of cells of type NA-, NA+, SR, and ML)
SR	percentage of small round cells (i.e., number of small round cells divided by total cells, where 'total cells' is the number of cells of type NA-, NA+, SR, and ML)
ML	percentage of leukocytes (i.e., number of leukocytes divided by total cells, where 'total cells' is the number of cells of type NA-, NA+, SR, and ML)
Age	age in years
Sex	male = 1, female = 0
Pack years	average cigarettes smoked per day times years smoked divided by 20
Lesion area	lesion area in mm^2 calculated using ellipse formula
Lichen planus	clinical impression of lichen planus--a binary measure completed by clinician at time of brush cytology sample collection indicating the presence ("1") or absence ("0") of the clinical features of lichen planus
Lesion color	variable indicating lesion color; white = 0, red = 1, red and white = 2

Appendix References

Abram TJ, Floriano PN, Christodoulides N, James R, Kerr AR, Thornhill MH, Redding SW, Vigneswaran N, Speight PM, Vick J et al. 2016. 'cytology-on-a-chip' based sensors for monitoring of potentially malignant oral lesions. Oral Oncology. 60:103-111.

Carpenter AE, Jones TR, Lamprecht MR, Clarke C, Kang IH, Friman O, Guertin DA, Chang JH, Lindquist RA, Moffat J et al. 2006. Cellprofiler: Image analysis software for identifying and quantifying cell phenotypes. Genome Biol. 7(10):R100.

Hemstreet GP, 3rd, Rao J, Hurst RE, Bonner RB, Waliszewski P, Grossman HB, Liebert M, Bane BL. 1996. G-actin as a risk factor and modulatable endpoint for cancer chemoprevention trials. J Cell Biochem Suppl. 25:197-204.

Huber MA. 2018. Adjunctive diagnostic techniques for oral and oropharyngeal cancer discovery. Dent Clin North Am. 62(1):59-75.

Lingen MW, Abt E, Agrawal N, Chaturvedi AK, Cohen E, D'Souza G, Gurenlian J, Kalmar JR, Kerr AR, Lambert PM et al. 2017. Evidence-based clinical practice guideline for the evaluation of potentially malignant disorders in the oral cavity: A report of the american dental association. J Am Dent Assoc. 148(10):712-727.

Pereira LHM, Reis IM, Reategui EP, Gordon C, Saint-Victor S, Duncan R, Gomez C, Bayers S, Fisher P, Perez A et al. 2016. Risk stratification system for oral cancer screening. Cancer Prev Res. 9(6):445.

Poate TWJ, Buchanan JAG, Hodgson TA, Speight PM, Barrett AW, Moles DR, Scully C, Porter SR. 2004. An audit of the efficacy of the oral brush biopsy technique in a specialist oral medicine unit. Oral Oncol. 40(8):829-834.

Rashid A, Warnakulasuriya S. 2015. The use of light-based (optical) detection systems as adjuncts in the detection of oral cancer and oral potentially malignant disorders: A systematic review. J Oral Pathol Med. 44(5):307-328.

Schneider CA, Rasband WS, Eliceiri KW. 2012. Nih image to imagej: 25 years of image analysis. Nat Methods. 9(7):671-675.

Sciubba JJ. 1999. Improving detection of precancerous and cancerous oral lesions: Computer-assisted analysis of the oral brush biopsy. J Am Dent Assoc. 130(10):1445-1457.

Speight PM, Abram TJ, Floriano PN, James R, Vick J, Thornhill MH, Murdoch C, Freeman C, Hegarty AM, D'Apice K et al. 2015. Interobserver agreement in dysplasia grading: Toward an enhanced gold standard for clinical pathology trials. Oral Surg Oral Med Oral Pathol Oral Radiol. 120(4):474-482.

Svirsky JA, Burns JC, Carpenter WM, Cohen DM, Bhattacharyya I, Fantasia JE, Lederman DA, Lynch DP, Sciubba JJ, Zunt SL. 2002. Comparison of computer-assisted brush biopsy results with follow up scalpel biopsy and histology. Gen Dent. 50(6):500-503.